Fabrication of Injectable Micro-Scale Opto-Electronically Transduced Electrodes (MOTEs) for Physiological Monitoring

Sunwoo Lee, *Member, IEEE*, Alejandro Javier Cortese, Aaron Mok, Chunyan Wu, Tianyu Wang, Ju Uhn Park, Conrad Smart, Shahaboddin Ghajari, *Member, IEEE*, Devesh Khilwani, Sanaz Sadeghi, *Member, IEEE*, Yanxin Ji, Jesse H. Goldberg, Chris Xu, Paul L. McEuen, and Alyosha Christopher Molnar, *Senior Member, IEEE*

***Abstract*— *In vivo*, chronic neural recording is critical to understand the nervous system, while a tetherless, miniaturized recording unit can render such recording minimally invasive. We present a tetherless, injectable micro-scale opto-electronically transduced electrode (MOTE) that is ∼60μm × 30μm × 330μm, the smallest neural recording unit to date. The MOTE consists of an AlGaAs micro-scale light emitting diode (μLED) heterogeneously integrated on top of conventional 180nm complementary metal-oxide-semiconductor (CMOS) circuit. The MOTE combines the merits of optics (AlGaAs μLED for power and data uplink), and of electronics (CMOS for signal amplification and encoding). The optical powering and communication enable the extreme scaling while the electrical circuits provide a high temporal resolution (<100μs). This paper elaborates on the heterogeneous integration in MOTEs, a topic that has been touted without much demonstration on feasibility or scalability. Based on photolithography, we demonstrate how to build heterogenous systems that are scalable as well as biologically stable – the MOTEs can function in saline water for more than six months, and in a mouse brain for two months (and counting). We also present handling/insertion techniques for users (*i.e.* biologists) to deploy MOTEs with little or no extra training. [2020-0080]**

***Index Terms*— CMOS post processing, electrophysiology, heterogenous integration, physiological monitoring, tetherless neural recording.**

Manuscript received April 21, 2020; accepted May 29, 2020. Date of publication June 12, 2020; date of current version October 7, 2020. This work was supported in part by the National Institutes of Health under Grant R21-EY027581 and Grant U01-NS107687, in part by the National Science Foundation under Grant ECCS-1542081, and in part by the National Science Foundation under Grant DMR-1120296. Subject Editor R. Ghodssi. *(Corresponding author: Sunwoo Lee.)*

Sunwoo Lee, Shahaboddin Ghajari, Devesh Khilwani, Sanaz Sadeghi, and Alyosha Christopher Molnar are with the Department of Electrical and Computer Engineering, Cornell University, Ithaca, NY 14853 USA (e-mail: sl933@cornell.edu; sg2367@cornell.edu; dk842@cornell.edu; ss3842@cornell.edu; am699@cornell.edu).

Alejandro Javier Cortese, Conrad Smart, Yanxin Ji, and Paul L. McEuen are with the Department of Physics, Cornell University, Ithaca, NY 14853 USA (e-mail: ajc383@cornell.edu; cs2239@cornell.edu; yj323@cornell.edu; plm23@cornell.edu).

Aaron Mok is with the Department of Biomedical Engineering, Cornell University, Ithaca, NY 14853 USA (e-mail: tm624@cornell.edu).

Chunyan Wu, Tianyu Wang, and Chris Xu are with the Department of Applied and Engineering Physics, Cornell University, Ithaca, NY 14853 USA (e-mail: cw674@cornell.edu; tw329@cornell.edu; cx10@cornell.edu).

Ju Uhn Park is with the Department of Computer Science, Cornell University, Ithaca, NY 14853 USA (e-mail: jp848@cornell.edu).

Jesse H. Goldberg is with the Department of Neurobiology and Behavior, Cornell University, Ithaca, NY 14853 USA (e-mail: jhg285@cornell.edu).

Color versions of one or more of the figures in this article are available online at http://ieeexplore.ieee.org.

Digital Object Identifier 10.1109/JMEMS.2020.2999496

I. Introduction

CHRONIC neural recording is crucial in gaining a better understanding of the brain and could provide insights in neurological disorders such as Alzheimer's Disease [1]. Although multi-electrode shanks are widely employed [2]–[4], they tend to generate ongoing damage and irritation due to relative motion between the implant and surrounding tissue [5]. Therefore, recent efforts have focused on building micro-scale, tetherless implants. While microscale RF [6]–[8] and ultrasonic [9]–[11] systems have shown promise, their transduction mechanisms make scaling below a millimeter challenging. On the other extreme, optical imaging based on calcium/voltage sensitive dyes/proteins allows noninvasive imaging at cell-scale resolution [1]. However, such optical imaging is limited by genetics to certain neurons and species, is impeded by scattering, and has a low temporal resolution. We present tetherless, injectable micro-scale opto-electronically transduced electrodes (MOTEs) which combine the merits of optical and electronic modalities to enable a) extreme scaling down to 60μm in cross-sectional diameter and b) direct electrical measurement with a high temporal resolution (<100μs). While circuit aspects of MOTEs have been present before [12], the challenges associated with heterogeneous integration and encapsulation are also significant in developing MOTEs, and are discussed here.

II. Theory

Heating in the brain dictates the maximum available optical power, where we have chosen infrared (IR) based on photo-voltaic (PV) efficiency and minimal absorption in the brain. Reference [13] has shown 160mW/mm^2 at the IR range to be the damage threshold. Our previous work has shown [12], [14] that a MOTE can function on a few microwatts of delivered power, so that it can function few

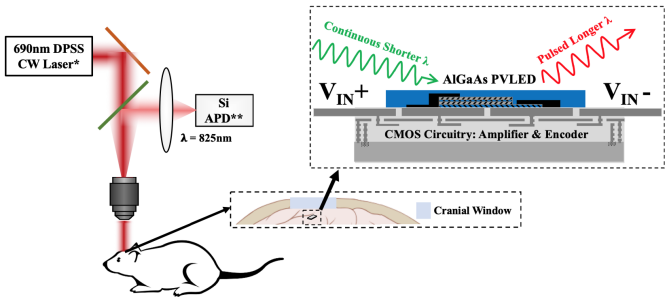

Fig. 1. A simplified schematic of MOTEs-based neural recording [12], [14]. ∗DPSS CW Laser: Diode-Pumped Solid-State Continuous Wavelength Laser. ∗∗Si APD: Silicon Avalanche Photodiode.

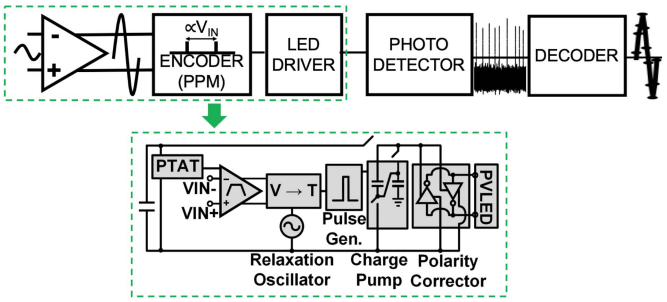

Fig. 2. System Block Diagram of a MOTE [12], [14].

millimeters deep in the brain through a transcranial window without exceeding 160mW/mm^2. The same work has shown that it is possible to build a circuit that can provide >10KHz bandwidth and ∼15μV$_{RMS}$ noise floor, using pulse-position-modulation (PPM) encoding, often used in energy starved systems such as satellites [15].

Fig. 1 shows a proof-of-concept illustration of the MOTE. The proposed system comprises of two parts: a) an optical component, a micro-scale (μ) AlGaAs diode that acts as both a PV for power transfer and as a light emitting diode (LED) for data communication (hence often referred as PVLED [16], [17]), and b) an electrical component, a complementary metal-oxide-semiconductor (CMOS) circuitry for electrical signal amplification and subsequent signal processing. We have chosen $\lambda_{Emission} = 825$nm and $\lambda_{Power} = 690$nm to optimize the PV efficiency while minimizing the brain absorption.

Fig. 2 shows a system-level block diagram for the MOTE circuitry [12], [14], and Fig. 3 illustrates an example of a MOTE operation – 500Hz, 500μV$_{PP}$ test signal is applied at the input differential electrodes, amplified and encoded into optical pulses, and finally detected by a photodetector (PD). The detected pulses' timing, namely their spacing (Δt), can then be used to recover the original sinusoid input.

While the MOTE's two main pillars, PVLED and the CMOS have individually been studied in detail [12], [14], [18], discussion of the associated integration challenges has been lacking. Given the MOTE's size scale, wire-bonding is out of the question for interconnecting PVLED and MOS: a single wire-bond-pad footprint is larger than the MOTE. Furthermore, such bendable wire-bonds jeopardize the insulation needed for chronic recording inside a biological medium. We have instead

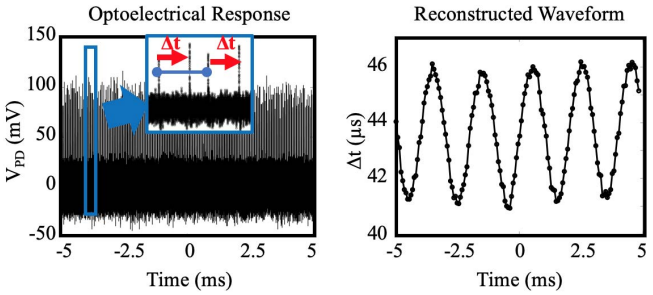

Fig. 3. A MOTE decoding example [12].

photolithographically integrated the PVLED and the CMOS to result in a scalable and robust system. We have optimized the polymer-based transfer method [18], [19] and dielectric cladding to allow MOTEs to survive in a mouse brain for two months (and counting). We also discuss a practical insertion method that has been lacking – a μ-pipette approach to allow users to manipulate and insert the MOTEs with a minimal learning curve.

III. Results

A. PVLED Transfer on CMOS

The following integration process is based on a 180nm foundry CMOS process, whose top metal is aluminum. A MOTE has four contact points: V$_{IN+}$, V$_{IN-}$, V$_{DD}$, and V$_{SS}$. The V$_{DD}$ and V$_{SS}$ are to be connected to the PVLED (*i.e.* anode and cathode) while the two input electrodes are to be coated with platinum for biocompatibility. Although it is crucial to have a planar surface for a successful PVLED transfer and its adhesion to the CMOS, a CMOS die is not chemical-mechanically polished (CMP) after its final dielectric deposition (*i.e.* the dielectric on top of the top metal) – instead, there is 1∼2μm of relief in the Si$_x$O$_y$N$_z$ dielectric on top of the top metal layer. Hence, we start the integration fabrication with CF$_4$ reactive ion etch (RIE) on the CMOS (Oxford 80: 150 W, 40 mTorr, 30 sccm CF$_4$) for about 30 minutes in total. This etch removes all the dielectric above the top metal while the aluminum acts as an etch stop (high selectivity against the CF$_4$ etch). It should be noted that 'pad opening' designation (the foundry selectively removes dielectric on top of the top metal for bondpads) is not used as the pad opening designation incurs 100∼200nm of unremovable (by the CF$_4$ etch) residues at the opening boundaries (suspected to originate from techniques used to make the openings at the foundry), detrimental to the subsequent PVLED transfer.

Following the dielectric removal, we transfer an AlGaAs μLEDs array that have been tailored to match the CMOS layout, using poly (methyl methacrylate) (PMMA) transfer techniques often used in 2D materials transfers [18], [19]. while both the V$_{DD}$ and the V$_{SS}$ aluminum pads are directly below the cathodic layer of the PVLED, they do not form ohmic contacts alleviating leakage concerns.

B. CMOS Integration

The transfer results in PVLED on CMOS with the PMMA still intact. To cleanly remove the PMMA, we employ a high

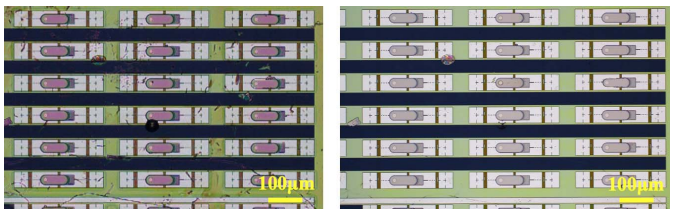

Fig. 4. AlGaAs μLEDs transferred on top of the MOTE CMOS die, before annealing (left) and after annealing (right).

vacuum annealing (Custom-built: 320°C for 2 hours at less than 10^{-6} Torr, 30-minute ramp from room temperature, and natural cool-down). This anneal not only removes the PMMA better than oxygen plasma it also enhances the adhesion between the CMOS and the μLEDs (simply using solvent to remove PMMA also washes the μLEDs off the CMOS surface). Post annealing, it is possible to rinse with solvent as well as deionized water (DI) to better remove polar residues for more than 15 minutes, further reducing the transfer process residues. Fig. 4 compares the before and the after the anneal. Importantly, any excess residues will later inhibit the cladding layer deposition and cause biological media to leak in.

After the annealing and the residue cleaning, ~90nm SiO_2 is deposited using atomic layer deposition (ALD) (Oxford FlexAL: 200°C, Plasma enhanced) to fill micro-cracks and voids, and further the adhesion of the PVLEDs on CMOS. We have found that a temperature lower than 200 °C results in SiO_2 with inadequate quality for cladding. Fig. 5 illustrates the ensuing fabrication steps based on four-mask contact lithography.

1) Contact: AZ® nLOF 2002 resist is used with ABM contact aligner to define contact openings. CHF_3/O_2 reactive ion etch (RIE) (Oxford 80: 200 W, 50 mTorr, 50 sccm CHF_3, 2 sccm O_2, 9 minutes) removes the ALD SiO_2 in the openings. Then buffered oxide etch (BOE, 6:1, 60 seconds) is used to remove naturally forming aluminum oxide, and form undercuts beneath the nLOF resist. Shortly after the BOE etch, the MOTE is placed inside a sputter for RF sputtering [20] (AJA: Base Pressure $< 10^{-6}$ Torr, RF = 50W, Ti ~ 5nm for adhesion, Pt ~ 50nm at 20mTorr), and lifted off in Shipley MICROPOSIT® REMOVER 1165.

2) Routing: AZ® nLOF 2002 resist is used again with the ABM contact aligner as in *1) contact openings*. Because there is no undercut this time, DC sputtering is used (AJA: Base Pressure $<10^{-6}$ Torr, Ti ~ 10nm for adhesion, Pt ~ 90nm at 20mTorr) and it is lifted off in the 1165 as before. There is a trade-off between the thickness of Pt (lower resistance) and the film stress & lift-off viability – we have found that ~100nm to be an optimal point. Also, because the routing metal has to cover uneven topologies, electron beam (e-beam) evaporation is not suitable for this step. Following the routing, ~10nm ALD Si_3N_4 (Oxford FlexAL: 350°C, Plasma enhanced) and ~90nm ALD SiO_2 (Oxford FlexAL: 200°C, Plasma enhanced) are deposited to insulate the routing metals. We find that the performance of MOTEs typically improves post the ALD deposition, likely owing to the thermal annealing effect during the step.

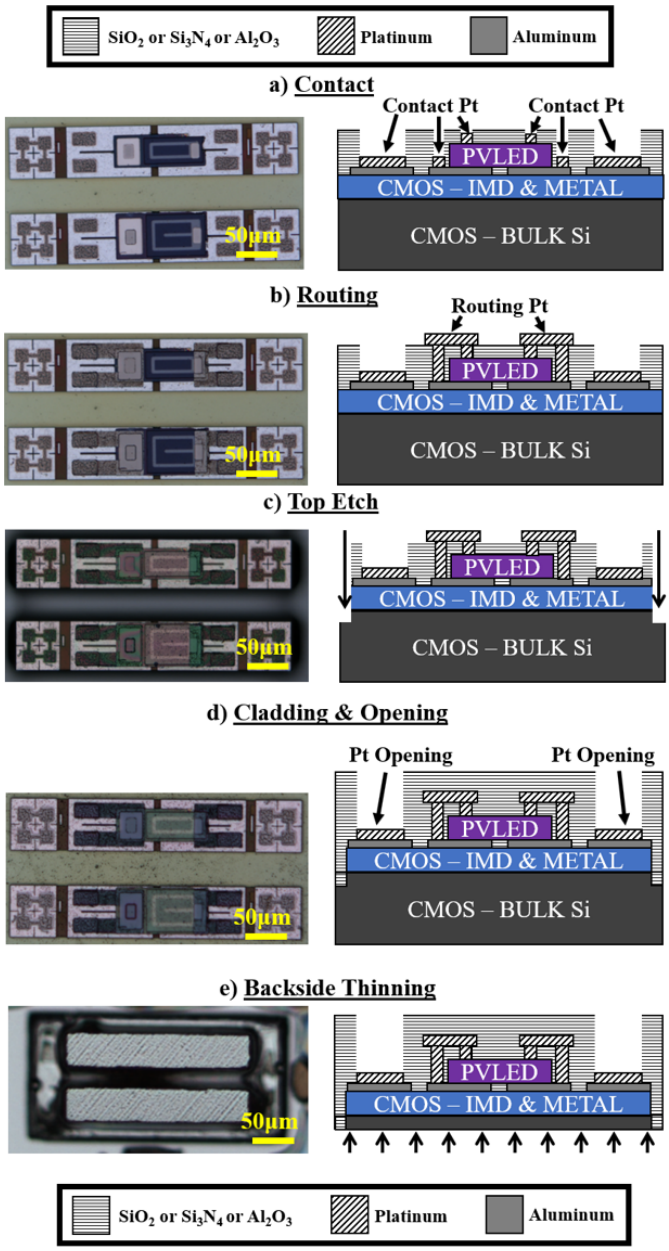

Fig. 5. MOTEs integration fabrication flow.

3) Top Etch: This step separates each MOTE in the array. Because we must etch through inter-metal dielectric (IMD) and into the bulk silicon, we use Cr hard mask to withstand the required prolonged etch. RF sputtering is used to deposit the Cr (AJA: Base Pressure $<10^{-6}$ Torr, RF = 50W, Cr ~ 100nm at 30mTorr). MEGAPOSIT™SPR™220-3.0 resist is used with the ABM contact aligner, and the Cr is selectively etched away using TRANSENE CHROMIUM ETCHANT 1020AC. After the Cr etch, the remaining resist is not stripped to serve as an additional etch mask to the Cr.

Inductively coupled plasma (ICP) RIE plasma etch is then used to etch the IMD (Oxford PlasmaPro 100 RIE: ICP = 3000W, RF = 60W, 4mTorr, 20sccm CH_2F_2, 80sccm He). While the ICP RIE provides excellent etch rate and vertical etch profile, it is difficult to guarantee sufficient

thermal cooling because the tool is made for four-inch wafers and larger, whereas CMOS die are typically on the order of millimeters. Therefore, we have employed a Si carrier wafer that is as thin as possible without being too fragile (four-inch, 400μm thick, double side polish (DSP) wafer) and attached our die using AI Technology, Inc. COOL-GREASE™(CGR7016). We have also programmed the etcher to cycle the etch (30s etch followed by 60s cooling). Even with the high power of the ICP RIE, ~1hr of etching time is required to remove the IMD, which is ~10μm of $Si_XO_YN_Z$.

We have noticed that the IMD color differs depending on whether the underlying bulk silicon is defined as diffusion layer or not during the tapeout. Hence, we have defined a section of the etch area to contain both the diffusion and non-diffusion area, so that it is optically apparent when the IMD is all etched away, and Si is exposed.

Following the IMD etch, we used deep-RIE (DRIE) (Unaxis 770 Deep Silicon Etcher) to etch away ~25μm of the bulk silicon. Together with the IMD thickness (~10μm), this defines the maximum thickness of MOTEs. This is because subsequent fabrication steps include thinning the backside silicon until the ~25μm deep trenches appear.

4) Cladding and Opening: Following *3) Top Etch*, both the remaining resist and the Cr are removed by oxygen plasma and the Cr Etch, respectively. Then, plasma enhanced chemical vapor deposition (PECVD) (OXFORD PlasmaPro 100 PECVD) is used to deposit ~200nm low stress Si_XN_Y (139MPa, Tensile) followed by ~900nm tetraethyl orthosilicate (TEOS) SiO_2. Furthermore, ~50nm ALD Al_2O_3 (Oxford FlexAL: 200°C, Plasma enhanced) is additionally deposited. While this cladding is needed to ensure longevity of the MOTEs inside biological media, input electrodes must be exposed. The photolithographic step is similar to the one shown in *c*) *Top Etch* – SPR330-2.0 atop sputtered Cr.

For the opening etch, the 3000W ICP RIE cannot be used as the extreme plasma density seems to damage the input capacitor in the CMOS circuitry. Therefore, we resorted to a lower power ICP RIE and a regular RIE which, while slower, are less damaging. We first etched away the Al_2O_3 using BCl_3/Ar ICP RIE (PlasmaTherm 770: ICP = 800W, RF = 15W, 7mTorr, 45sccm BCl_3, 5sccm Ar), followed by CHF_3/O_2 RIE etch (Oxford 80: 240W, 40mTorr, 50sccm CHF_3, 2sccm O_2) to remove the remaining dielectric. The same etching is then repeated on the backside of the MOTEs chip as the conformal nature of the ALD and PECVD often leads to the unwanted dielectric deposition on the backside. Then the SPR220 photoresist and Cr are removed as in *3) Top Etch*.

5) Backside Thinning: The final step, thinning, is done through DRIE (Unaxis 770 Deep Silicon Etcher), which while being efficient in terms of the etch rate, suffers from the same issues as the ICP RIE during IMD etch – heating and handling. While Cornell NanoScale Facility (CNF) possesses higher power (hence faster etch) DRIE (PlasmaTherm Deep Silicon Etcher: 3000W vs. 800W of the Unaxis), we opted for the lower power Unaxis due to heating concerns. Therefore, we first spun the SPR 330-2.0 resist on a 400μm thick DSP wafer, and before the resist bake, the MOTEs die is placed upside down against the freshly spun resist, and gently pressed before being baked for twice the typical soft-bake time. Lastly, DRIE (Unaxis 770 Deep Silicon Etcher) is used in cycles, 40 loops at a time (follow by 30 seconds of cooling on a room temperature chill plate) to minimize the excess heating, until the trenches defined in the *c*) *Top Etch* appear.

Fig. 6. A scanning electron microscope (SEM) image of a fully released MOTE.

TABLE I
A YIELD TABLE OF MOTES FABRICATION

MOTE_V5_C24	1	2	3	4	5	6	7	8	9
1									
2									
3									
4									
5									
6									
7									
8									
9									
10									

CMOS Platform	90	**Dead Devices**	14.00
uLED Trasnferred on	90	**Alive Devices**	76.00
Transfer Yield (%)	100	**Total Yield (%)**	84.44

It is important to note that if there are any residues present in between the CMOS and the μLEDs, then the heating is exacerbated and the MOTEs can be destroyed during this DRIE or ICP RIE etching for *3) Top Etch*, as the authors found, painfully, prior to the adaptation of the high vacuum annealing.

Once the trenches appear, we immerse the MOTEs on the carrier wafer in acetone, and through medium exchange, the MOTEs are transferred to isopropanol, and finally to sterile water. Fig. 6 shows a fully released MOTE post the integration fabrication.

Table 1 describes the yield of the integration fabrication from the latest run. As shown, the μLEDs transfer is often perfect (the transfer yield rarely drops below 90%), and most failures are likely incurred during the integration fabrication. Though μLEDs may get damaged (*i.e.* micro cracks) during the transfer, this is hard to ascertain at the time of transfer.

An interesting phenomenon we have noticed is that once the MOTEs are released, and in a solution (*i.e.* saline), if there are any cracks in the encapsulation, inorganic 'black mold' quickly appears upon exposure to light. We speculate that this is likely due to an unwanted electrochemical interactions powered by the PVLED. Micro-bubbles near the cracks can

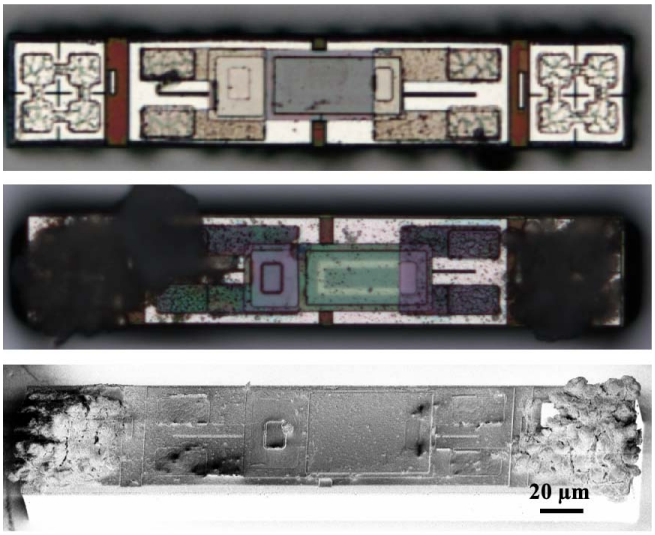

Fig. 7. Successful encapsulation (top) vs. defective encapsulation (middle). The bottom is a SEM image of the middle.

also be observed during such failure processes – typically the micro-bubble sites quickly turn into 'black mold' sites. Fig. 7 compares a successful MOTE against its defective counterpart.

IV. Handling and Insertion

Once the MOTEs are in a sterile solution, individual MOTEs are nearly invisible to a naked eye, making them extremely difficult to handle. We have found using μ-pipettes (with fiber) under a stereoscope (Thermo Fisher Scientific Fisher Stereomaster F1411-D830-002) to be the most straightforward method to handle and insert MOTEs. Once a μ-pipette is inserted near a MOTE in solution, capillary forces draw solution into the pipette, along with a MOTE. The μ-pipette tip can then be placed in contact with a paper wipe (we have used Kimberly-Clark Kimtech Science Kimwipes), and as the wipe absorbs solution inside the μ-pipette, the MOTE will be brought to the tip of the pipette. Thanks to the light weight of the MOTE ($\sim 1\mu$g), the van der Waals attraction between the μ-pipette and the MOTE is enough to keep the MOTE intact inside the now-dry μ-pipette while moving.

To insert the MOTE into the brain, we have affixed the MOTE-containing μ-pipette to a X-Y-Z micro-positioner and inserted a stainless-steel wire into the μ-pipette as a push mechanism. Once the cranial opening is made, the μ-pipette is brought to touch down on dura. Because a MOTE is similar to a razorblade in its dimensions, it is possible to puncture the dura with the MOTE (*i.e.* the μ-pipette, which is bigger than the MOTE, stays outside dura, minimizing the insertion damage). Fig. 8 depicts the insertion scheme and a *in vivo* insertion into a mouse brain.

Each MOTE insertion can take as little as five minutes after a few practice sessions, and we have routinely implanted four to eight MOTEs each surgery. Once the MOTEs are inserted, a head bar window is installed to allowed for awake neural recording. Fig. 9 shows a mouse with the head bar and a typical *in vivo* measurement setup. While we have yet to obtain a

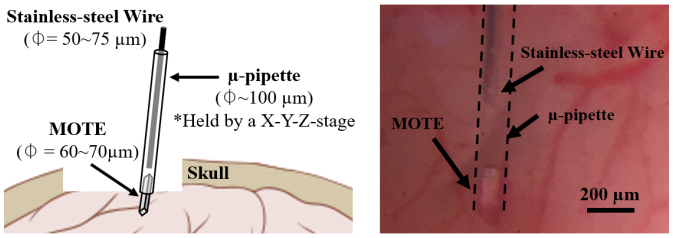

Fig. 8. A MOTE insertion using a pulled μ-pipette. The left shows a simplified insertion mechanism while the right shows an *in vivo* insertion.

Fig. 9. A mouse with a head bar window, ~2 months after the insertion surgery (left). The right shows the mouse (awake) under measurement using a head-bar fix apparatus.

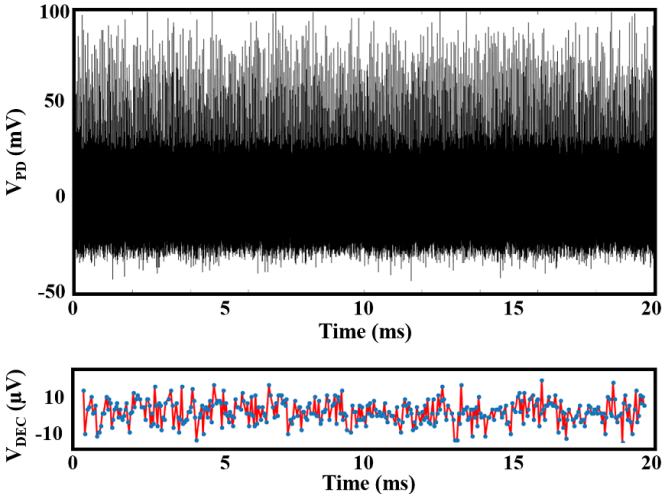

Fig. 10. A MOTE measurement *in vivo*. While the decoded signal (bottom) did not show a neural response, the observed optical pulses (top) indicate that the MOTE is functioning as designed.

neural signal from the MOTE (as inserting MOTEs near active neurons is largely chance based), Fig. 10 demonstrates that the inserted MOTEs are functioning properly, outputting pulses (insertion depth $\sim 200\mu$m, optical power ~ 23mW/mm^2).

V. Conclusion

For chronic, tetherless neural recording, MOTEs provide a compelling alternative to existing modalities such as electrodes shanks and coils/ultrasound-based implants. The heterogenous integration described in this manuscript has not only enabled the MOTE to be scaled down below human hair width, but also enabled the MOTEs to be fabricated en masse with high yield, proving scalability of the technology. Table II compares the MOTEs against state-of-the-arts.

TABLE II
TABLE OF COMPARISON

	Integrated Neural Interface [6]	Microwave Backscattering [21]	Neural Dust [11]	MOTE [This Work]
Wireless Power Source	RF Coil	RF	Ultrasonic	Optical
Technology (nm)	500	-	65	180
Gain (dB)	60	-	24	24
Bandwidth (KHz)	5	5	5	10
Noise Floor (μV_{RMS})	5.1	63	5.3	15
Power	135µW	0	37.7	<1µW
Cross-sectional Diameter	>300µm	>10mm	>500µm	>57µm
Volume per Channel (mm^3)	>10	360	0.8	$<1x10^{-3}$
Functional Depth (mm)	Surface Only	Surface Only	50	<5 (est.)
Functional Depth/Volume per Channel (mm^{-2})	-	-	61.7	$<5x10^3$

MOTEs can survive in biological media for months timescale, can easily be integrated with standard microscopy systems, and can be handled with μ-pipettes that many biologists are familiar with. Furthermore, the proposed fabrication and handling methodologies are applicable to other types of heterogeneously integrated CMOS systems.

ACKNOWLEDGMENT

The authors would like to thank H. Wang, S. Chae, J. Choi, and C. Lee for critical discussions. This work was performed in part at the Cornell NanoScale Facility, a member of the National Nanotechnology Coordinated Infrastructure, and made use of the Cornell Center for Materials Research Facilities.

REFERENCES

[1] A. P. Alivisatos, M. Chun, G. M. Church, R. J. Greenspan, M. L. Roukes, and R. Yuste, "The brain activity map project and the challenge of functional connectomics," *Neuron*, vol. 74, no. 6, pp. 970–974, Jun. 2012.

[2] G. Buzsáki *et al.*, "Tools for probing local circuits: High-density silicon probes combined with optogenetics," *Neuron*, vol. 86, no. 1, pp. 92–105, Apr. 2015.

[3] Q. Bai, K. D. Wise, and D. J. Anderson, "A high-yield microassembly structure for three-dimensional microelectrode arrays," *IEEE Trans. Biomed. Eng.*, vol. 47, no. 3, pp. 281–289, Mar. 2000.

[4] F. Michon *et al.*, "Integration of silicon-based neural probes and microdrive arrays for chronic recording of large populations of neurons in behaving animals," *J. Neural Eng.*, vol. 13, no. 4, Jun. 2016, Art. no. 046018.

[5] D. H. Szarowski *et al.*, "Brain responses to micro-machined silicon devices," *Brain Res.*, vol. 983, nos. 1–2, pp. 23–35, Sep. 2003.

[6] R. Harrison *et al.*, "A low-power integrated circuit for a wireless 100-electrode neural recording system," in *IEEE Int. Solid-State Circuits Conf. (ISSCC) Dig. Tech. Papers*, San Francisco, CA, USA, May 2006, pp. 2258–2267.

[7] Z. Jiang *et al.*, "TaiNi: Maximizing research output whilst improving animals' welfare in neurophysiology experiments," *Sci. Rep.*, vol. 7, no. 1, Dec. 2017, Art. no. 8086.

[8] S. B. Lee, B. Lee, M. Kiani, B. Mahmoudi, R. Gross, and M. Ghovanloo, "Fabrication and microassembly of a mm-sized floating probe for a distributed wireless neural interface," *IEEE Sensors J.*, vol. 16, no. 2, pp. 475–484, Jan. 2016.

[9] D. Seo, J. M. Carmena, J. M. Rabaey, E. Alon, and M. M. Maharbiz, "Neural dust: An ultrasonic, low power solution for chronic brain-machine interfaces," 2013, *arXiv:1307.2196*. [Online]. Available: http://arxiv.org/abs/1307.2196

[10] D. Seo *et al.*, "Wireless recording in the peripheral nervous system with ultrasonic neural dust," *Neuron*, vol. 91, no. 3, pp. 529–539, Aug. 2016.

[11] M. M. Ghanbari *et al.*, "A Sub-mm3 ultrasonic free-floating implant," *IEEE J. Solid-State Circuits*, vol. 54, no. 11, pp. 3017–3030, Dec. 2019.

[12] S. Lee, A. J. Cortese, A. P. Gandhi, E. R. Agger, P. L. McEuen, and A. C. Molnar, "A 2500 μm 57 $\times$m microscale opto-electronically transduced electrodes (MOTEs) for neural recording," *IEEE Trans. Biomed. Circuits Syst.*, vol. 12, no. 6, pp. 1256–1266, Dec. 2018.

[13] K. Podgorski and G. Ranganathan, "Brain heating induced by near-infrared lasers during multiphoton microscopy," *J. Neurophysiology*, vol. 116, no. 3, pp. 1012–1023, Sep. 2016.

[14] S. Lee, A. J. Cortese, P. Trexel, E. R. Agger, P. L. McEuen, and A. C. Molnar, "A 330μm$\times$90μm opto-electronically integrated wireless system-on-chip for recording of neural activities," in *IEEE Int. Solid-State Circuits Conf. (ISSCC) Dig. Tech. Papers*, San Francisco, CA, USA, Feb. 2018, pp. 292–294.

[15] H. Hemmati, A. Biswas, and I. B. Djordjevic, "Deep-space optical communications: Future perspectives and applications," *Proc. IEEE*, vol. 99, no. 11, pp. 2020–2039, Nov. 2011.

[16] I. Haydaroglu and S. Mutlu, "Optical power delivery and data transmission in a wireless and batteryless microsystem using a single light emitting diode," *J. Microelectromech. Syst.*, vol. 24, no. 1, pp. 155–165, Feb. 2015.

[17] I. Haydaroglu, M. T. Ozgun, and S. Mutlu, "Optically powered optical transmitter using a single light-emitting diode," *IEEE Trans. Circuits Syst. I, Reg. Papers*, vol. 64, no. 8, pp. 2003–2012, Aug. 2017.

[18] A. J. Cortese *et al.*, "Microscopic sensors using optical wireless integrated circuits," *Proc. Nat. Acad. Sci. USA*, vol. 117, no. 17, pp. 9173–9179, Apr. 2020.

[19] X. Li *et al.*, "Large-area synthesis of high-quality and uniform graphene films on copper foils," *Science*, vol. 324, no. 5932, pp. 1312–1314, Jun. 2009.

[20] Y. Homma and S. Tsunekawa, "Planar deposition of aluminum by RF/DC sputtering with RF bias," *ECS J. Solid State Sci. Technol.*, vol. 132, no. 6, pp. 1466–1472, 1985.

[21] A. Kiourti, C. W. L. Lee, J. Chae, and J. L. Volakis, "A wireless fully passive neural recording device for unobtrusive neuropotential monitoring," *IEEE Trans. Biomed. Eng.*, vol. 63, no. 1, pp. 131–137, Jan. 2016.

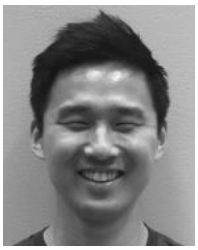

Sunwoo Lee (Member, IEEE) received the B.S. degree in electrical and computer engineering from Cornell University, Ithaca, NY, USA, in 2010, and the M.S. and Ph.D. degrees in electrical engineering from Columbia University, NY, in 2012 and 2016, respectively, working graphene-based nano-electromechanical systems for signal processing and sensing applications.

In April 2016, he joined the Molnar Group as a Post-Doctoral Researcher at the School of Electrical and Computer Engineering, Cornell University, to work on opto-electrically transduced micro-scale neural interfaces.

Alejandro Javier Cortese received the B.S. degree (Hons.) in physics and the B.S. degree in mathematics from Duke University, Durham, NC, USA, in 2012, and the M.S and Ph.D. degrees in physics from Cornell University, Ithaca, NY, USA, in 2015 and 2019, respectively. He is currently a Presidential Postdoctoral Fellow with Cornell University, working on wireless optoelectronic sensors.

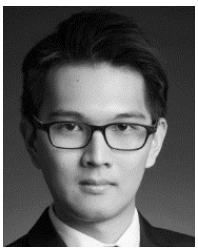

Aaron Mok received the B.B.A. degree in marketing and the B.Eng. degree in medical engineering from The University of Hong Kong, and the M.Phil. degree in electrical and electronic engineering under the supervision of Dr. Kevin Tsia. He is currently pursuing the Ph.D. degree in biomedical engineering with Cornell University, under the supervision of Prof. Chris Xu. He is interested in the development of neurotechnology, with a focus on advancing optical tools to image and study neuroactivities.

Chunyan Wu received the B.S. degree in bioengineering and biomedical engineering from the Hefei University of Technology in 2012 and the M.Eng. degree in biomedical engineering from Cornell University in 2014, where she is currently pursuing the Ph.D. degree in biomedical engineering.

Tianyu Wang studied applied physics from Shanghai Jiao Tong University. He received the B.S. degree in biological and environmental engineering from Cornell University, Ithaca, NY, USA, in 2012, and the Ph.D. degree in applied engineering physics from Cornell University in 2018, during which period he developed three-photon calcium imaging technology. He is currently a Mong Senior Cornell Neurotech Fellow, and a Post-Doctoral Researcher working on optical computing with the McMahon Lab, Cornell University.

Ju Uhn (Mike) Park is currently pursuing the master's degree in computer science and minoring with the Policy Analysis and Management, Cornell University, Ithaca, NY. He joined the Molar Group in June 2019 to develop a graphical user interface for microscale opto-electronically transduced electrodes (MOTEs) system.

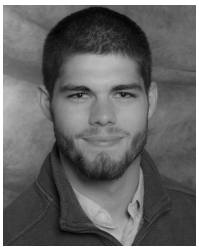

Conrad Smart received the B.S. degree in physics and mathematics from the University of Louisville, Louisville, KY, USA, in 2017. He is currently pursuing the Ph.D. degree in physics with Cornell University, Ithaca, NY, USA.

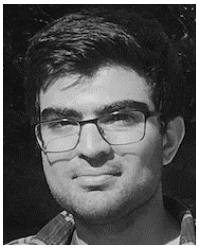

Shahaboddin Ghajari (Member, IEEE) received the B.S. degree from the Ferdowsi University of Mashhad, Mashhad, Iran, and the M.S. degree in electrical engineering from the Sharif University of Technology, Tehran, Iran, in 2015 and 2017, respectively. He is currently pursuing the Ph.D. degree in electrical and computer engineering with the Molnar Group, Cornell University, Ithaca, NY, USA.

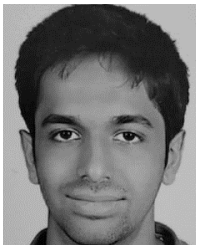

Devesh Khilwani received the B.Tech. and M.Tech. degrees in electrical engineering from IIT Bombay, India, in 2019. He is currently pursuing the master's degree with the Molnar Group, School of Electrical and Computer Engineering, Cornell University, Ithaca, NY, USA, working on biosensors.

Sanaz Sadeghi (Member, IEEE) received the B.Sc. and M.Sc. degrees in electrical engineering from the Sharif University of Technology, Tehran, Iran, in 2015 and 2017, respectively. She is currently pursuing the Ph.D. degree in electrical and electronics engineering with the Molnar Group, Cornell University, Ithaca, NY, USA.

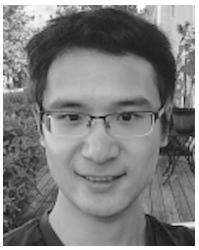

Yanxin Ji received the B.S. degree in physics from Peking University, Beijing, China, in 2014. He is currently pursuing the Ph.D. degree in physics with Cornell University, Ithaca, NY, USA, working on 2D materials sensors.

Jesse H. Goldberg received the B.S. degree from the Haverford College and the M.D. and Ph.D. degrees from Columbia University. His Ph.D. degree with Rafa Yuste focused on dendritic computation and microcircuits of the cerebral cortex. In medical school, he became interested disorders such as Parkinson's and dystonia that impair basal ganglia dependent reinforcement learning. His postdoctoral work at MIT focused on how the basal ganglia implement RL in juvenile songbirds. His lab combines high channel count awake-behaving electrophysiology, closed-loop optogenetics, and machine learning-guided behavioral analysis to study how animals learn through practice. He has been supported by the Pew, Klingenstein, Kavli, NIH New Innovator, and Cornell Neurotech. His guiding philosophy is that comparative approaches (across species and across the animal-machine divide) are necessary to distinguish general principles from behavior-, effector-, machine-, and species-specific solutions to motor learning problems.

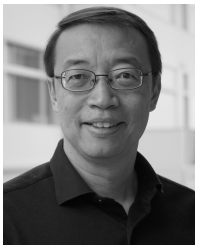

Chris Xu received the B.S. degree in physics from Fudan University, Shanghai, China, and the Ph.D. degree in applied physics from Cornell University. He is currently a Professor with the Applied and Engineering Physics, Cornell University, the Mong Family Foundation Director of Cornell Neurotech – Engineering, and the Director of the Cornell NeuroNex Hub, an NSF funded center for developing neurotechnology. Prior to Cornell, he was a member of technical staff at Bell Laboratories, where he developed new long haul fiber optic communication systems. His current research areas are biomedical imaging and fiber optics. He is a fellow of the Optical Society of America, and a fellow of the National Academy of Inventors.

Paul L. McEuen received the B.S. degree in engineering physics from the University of Oklahoma, Norman, OK, USA, in 1985, and the Ph.D. degree in applied physics from Yale University, New Haven, CT, in 1991.

From 1990 to 1991, he worked as a Post-Doctoral Researcher at MIT, Cambridge, MA, USA, before joining the faculty of the University of California, Berkeley, CA, USA. He moved to Cornell University in 2001, where he is currently the Goldwin Smith Professor of physics. He is a member of the National Academy of Sciences and an American Physical Society fellow.

Alyosha Christopher Molnar (Senior Member, IEEE) received the B.S. degree (Hons.) in engineering from the Swarthmore College, Swarthmore, PA, USA, in 1997, and the M.S. and Ph.D. degrees in electrical engineering from the University of California, Berkeley, CA, USA, in 2003 and 2007, respectively. From 1998 to 2002, he was with the RF IC Group, Conexant Systems, Inc. (now Skyworks Solutions, Inc.), Newport Beach, CA, where he developed their first-generation GSM direct conversion receiver. In August 2007, he joined the faculty of the School of Electrical and Computer Engineering, Cornell University, Ithaca, NY, USA.